

A New Hole Transport Material for Efficient Perovskite Solar Cells With Reduced Device Cost

Yuhao Sun, Changlei Wang, Dewei Zhao,* Jiangsheng Yu, Xinxing Yin, Corey R. Grice, Rasha A. Awni, Niraj Shrestha, Yue Yu, Lei Guan, Randy J. Ellingson, Weihua Tang,* and Yanfa Yan*

To realize commercialization of perovskite solar cell (PVSC) technology, it is essential to reduce the device costs while maintaining high power conversion efficiencies (PCEs). So far, the high cost of the most commonly used hole selective material, 2,2',7,7'-Tetrakis (N,N-di-p-methoxyphenylamino)-9,9'-spiro-bifluorene (spiro-OMeTAD), for high-PCE PVSCs presents a significant obstacle for device cost reduction. In this work, the synthesis and characterization of a new spiro-OMeTAD derivative hole selective material, 2,6,14-tris(5'-(N,N-bis(4-methoxyphenyl)aminophenol-4-yl)-3,4-ethylenedioxythiophen-2-yl)-tritycene (TET) is reported. TET features a three-dimensional structure consisting of a triptycene core and triarylamine arms linked by 3,4-ethylenedioxythiophene, facilitating efficient hole transport. Planar PVSCs using TET hole selective layers (HSLs) achieved high fill factors of over 81% and steady-state efficiencies of up to 18.6%, comparable with that (19.0%) of PVSC using spiro-OMeTAD HSL. Importantly, the hereby reported efficient PVSCs can be produced with very thin TET HSLs (about 30 nm). Considering the lower laboratory synthesis and purification cost (\$123 vs. \$500 g⁻¹) and thinner HSL (30 vs. 200 nm), the cost for TET on a unit area of one device is 25 times lower than that for high-purity spiro-OMeTAD. The device with TET HSL shows good stability under continuous illumination. Therefore, this work makes a significant step forward toward the commercialization of the emerging PVSC technology.

coefficient, tunable bandgaps, long carrier lifetime, and long carrier diffusion length.^[1–6] Perovskite solar cells (PVSCs) have been anticipated as a promising photovoltaic technology to produce low-cost solar electricity owing to their rapid increase in record power conversion efficiencies (PCEs) certified to over 22% in the past few years, low-cost solution processing at low temperatures, and compatibility with roll-to-roll manufacturing on plastic substrates.^[7–19] Their unique optoelectronic properties have also made metal halide perovskites attractive in other fields such as light-emitting diodes (LEDs),^[20–22] photo-detectors,^[23,24] and lasers.^[25]

PVSCs typically use electron selective layers (ESLs) and hole selective layers (HSLs) to discriminately block or transport certain photogenerated charges. An ESL blocks holes and transports electrons, while an HSL blocks electrons and transports holes. High-performance PVSCs are usually made by inserting a perovskite layer in between an ESL and an HSL. Besides the quality of perovskite absorber layer, the properties of ESLs and HSLs can significantly affect the performance of the resulting PVSCs. Requirements for an ideal HSL (ESL) material include^[10,26–31]:

1. Introduction

Organic-inorganic hybrid metal-halide perovskites have shown unique photovoltaic properties such as high absorption

Y. Sun, Dr. J. Yu, X. Yin, Prof. W. Tang
Key Laboratory of Soft Chemistry and Functional Materials (Ministry of Education of China)
Nanjing University of Science and Technology,
Nanjing, 210094, China
Email: whtang@njjust.edu.cn

C. Wang, Dr. D. Zhao, C. R. Grice, R. A. Awni, N. Shrestha, Y. Yu, L. Guan, Prof. R. J. Ellingson, Prof. Y. Yan
Department of Physics and Astronomy and Wright Center for Photovoltaics Innovation and Commercialization
The University of Toledo,
Toledo, OH 43606, US
E-mail: dewei.zhao@utoledo.edu; yanfa.yan@utoledo.edu

DOI: 10.1002/solr.201700175

1) a bandgap value is wide enough such that it does not significantly absorb visible light, reducing photocurrent loss; 2) the highest occupied molecular orbital (HOMO) level (lowest unoccupied molecular orbital, LUMO, level of ESL) should be slightly higher (lower) in energy than the valence band maximum (VBM) (conduction band minimum, CBM) of perovskite absorber to facilitate hole (electron) transfer; 3) the LUMO level (HOMO level of ESL) should be much higher (lower) in energy than the CBM (VBM) of perovskite to block electrons (holes) from approaching the interface with the perovskite layer to prevent charge recombination; and 4) a modest hole (electron) conductivity is required to effectively transport charges and achieve balanced charge transport through the PVSC.

Currently, high-PCE PVSCs use metal oxides as ESLs, such as TiO₂,^[10,32] SnO₂,^[13,14,33] and BaSnO₃,^[34] and organic

materials as HSLs,^[26,27] such as 2,2',7,7'-Tetrakis (N,N-di-p-methoxyphenylamino)-9,9'-spirobifluorene (spiro-OMeTAD),^[10] poly[bis(4-phenyl)-(2,4,6-trimethylphenyl)amine] (PTAA),^[34-36] and 2',7'-bis(bis(4-methoxyphenyl)amino)spiro[cyclopenta[2,1-b:3,4-b']dithiophene-4,9'-fluorene] (FDT),^[32] spiro[fluorene-9,9'-xanthene] based HSL termed X60,^[37] V862,^[38] Trux-OMeTAD.^[39] Inorganic HSLs, such as NiOx,^[40,41] CuSCN,^[42,43] CuI^[44] have also been explored as HSLs for PVSCs. Spiro-OMeTAD is the most commonly used HSL material for fabricating efficient PVSCs. It is an excellent hole transport material since it meets the requirements for an ideal HSL material. However, the use of spiro-OMeTAD may seriously hinder the commercialization of the PVSC technology because of the following shortfalls: 1) it has a high synthesis and purification cost;^[32,45] 2) it must be sufficiently thick, typically about 200 nm, in order to achieve high PCEs, which is much thicker than other HSLs and thus more material usage;^[46] and 3) it requires oxygen doping, which is incompatible with device encapsulation.^[47,48] Therefore, it is urgently necessary to design and demonstrate new spiro-OMeTAD derivatives or alternatives that can overcome these shortfalls, while maintaining high PCEs, to further reduce the material cost barriers to PVSC commercialization.

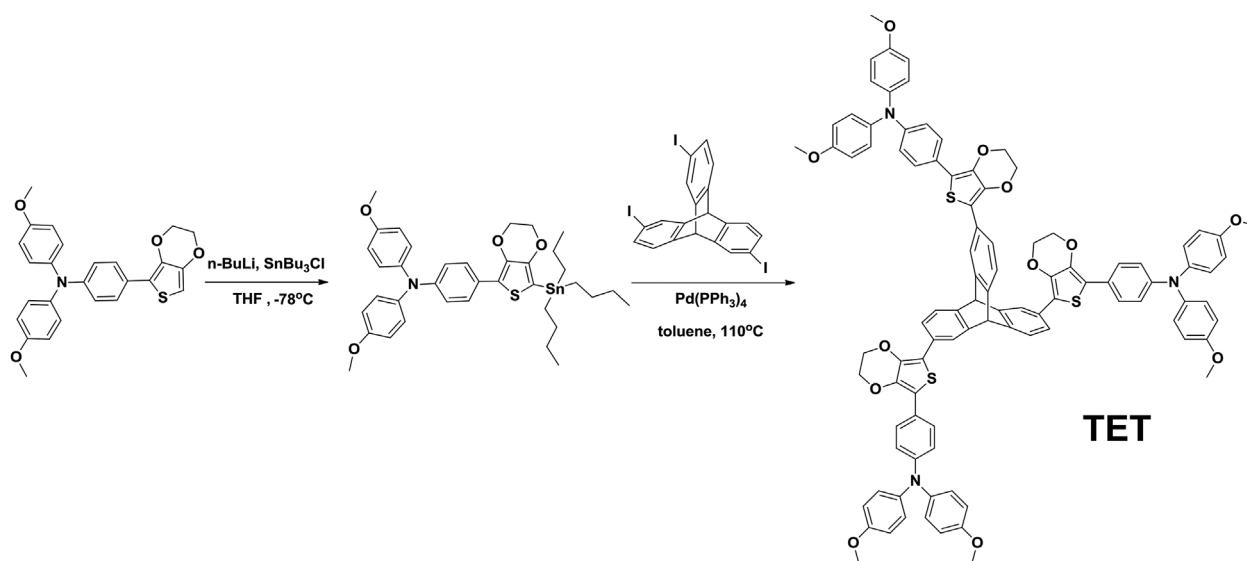
Here, we design and synthesize a new star-shaped oligomer, a spiro-OMeTAD derivative, 2,6,14-tris(5'-(N,N-bis(4-methoxyphenyl)aminophenyl)-3,4-ethylenedioxythiophen-2-yl)-tritycene (TET) (see **Scheme146\1**), which features a triptycene core and triarylamine arms linked by 3,4-ethylenedioxythiophene moiety, leading to proper HOMOs and high hole mobility. As a promising HSL, TET inherits the outstanding optoelectronic properties of spiro-OMeTAD while overcoming the aforementioned shortfalls. PVSCs using TET HSLs have achieved a maximum PCE of 19.1% under reverse voltage scan and steady-state efficiency of 18.6%, comparable with those of PVSCs using spiro-OMeTAD HSLs (19.5% PCE and 19.0% steady-state efficiency). The laboratory synthesis and purification cost of TET is estimated to be about \$123 g⁻¹ (see cost calculation

for TET in Supporting Information), one quarter of that of spiro-OMeTAD (about \$500 g⁻¹).^[32] More importantly, our high-PCE PVSCs are produced with very thin TET films (≈ 30 nm), which is about one order of magnitude thinner than the typical thickness of spiro-OMeTAD (≈ 200 nm) or FDT (≈ 170 nm) HSLs. Taking this into account, the unit cost of TET used in PVSCs is roughly one 25th of that of spiro-OMeTAD and one third of that of FDT.^[32] Additionally, TET as an HSL does not require oxygen doping and the PVSCs using TET HSL show good stability under continuous illumination. Meanwhile, the high solubility in environmentally friendly toluene makes the TET deposition easier for large-scale industrial manufacturing. Therefore, our TET HSL provides an important step forward toward commercialization of the emerging PVSC technology.

2. Results and Discussion

The synthetic procedure of TET is illustrated in Scheme146\1 and experimental details are given in Supporting Information. TET was synthesized using Stille coupling reaction between 2,6,14-triiodotriptycene and 4-methoxy-N-(4-methoxyphenyl)-N-(4-(7-(tri-butylstannyl)-2,3-dihydrothieno[3,4-b][1,4]dioxin-5-yl)phenyl)aniline. The iodotriptycene was prepared via a three-step approach including nitration, ammoniation, and iodination of triptycene. The 4-methoxy-N-(4-methoxyphenyl)-N-(4-(7-(tri-butylstannyl)-2,3-dihydrothieno[3,4-b][1,4]dioxin-5-yl)phenyl)aniline was constructed via a Stille coupling between 3,4-ethylenedioxythiophene (EDOT) and N,N-bis(4-methoxyphenyl)aniline. Thus, the TET features a triptycene core and triarylamine arms linked by EDOT. Such a three-dimensional (3D) structure in TET would facilitate efficient hole transport. After column chromatography purification and recrystallization from methanol, the analytically pure TET was produced for PVSC fabrication.

More importantly, our star shaped TET HSL shows good solubility in several common organic solvents, such as toluene



Scheme 1. Synthetic route for the preparation of TET.

and chlorobenzene, which is especially useful for solution-processed HSL deposition. It is worth highlighting that the high solubility in toluene makes the deposition of TET environmentally friendly, compared with chlorobenzene, and therefore, suitable for industrial manufacturing. The chemical structure of TET was successfully characterized using nuclear magnetic resonance (NMR) (Figure S1-11, ¹H, ¹³C, Supporting Information) and matrix assisted laser desorption/ionization-time of flight (MALDI-TOF) mass spectrometry (Figure S12, Supporting Information).

Thermogravimetric analysis (TGA) of TET in nitrogen revealed that TET exhibits a good thermal stability up to 404 °C, with 5% weight loss observed till 404 °C (Figure S13, Supporting Information). This value is comparable with that of FDT (400 °C) and spiro-OMeTAD (445 °C).^[32]

Figure 1a shows the absorption and photoluminescence (PL) spectra of a TET film. Its maximum absorption peak is located at 394 nm and the absorption onset is at around 446 nm, leading to an estimated optical bandgap (E_g) of 2.78 eV. The PL emission spectrum of TET displays a maximum centered at 481 nm. Cyclic voltammetry (CV) was employed to evaluate the HOMO and LUMO levels of pristine TET, and ferrocene/ferrocenium (Fc/Fc⁺) was used as the internal standard, with the formal potential of Fc/Fc⁺ measured as 0.48 V versus Ag/AgCl electrode. As shown in the inset of Figure 1a, a clear oxidation peak is observed for TET. From the onset potential for oxidation, the HOMO level of TET was determined to be -5.08 eV, close to that of spiro-OMeTAD.^[32] Taking the optical E_g of 2.78 eV for TET into account, the LUMO level of TET can be estimated to be -2.30 eV. The VBM level of our perovskite absorber, MA_{0.7}FA_{0.3}PbI₃ (MA = methylammonium and FA = formamidinium), is \approx -5.40 eV,^[13,36,49] which indicates that TET has energetics favorable for hole transfer from this material.

The electronic structures of TET and spiro-OMeTAD were further calculated by density functional theory (DFT), with their energy levels shown in Figure 1b. The DFT calculation was carried out using Gaussian program at the B3LYP/6-31G (d,p) level. Both TET and spiro-OMeTAD show electron density delocalized on the whole molecules for HOMO; while the LUMO mainly localizes on the triphenylamine and EDOT units for TET and the central spirobifluorene-group for spiro-OMeTAD. For

TET, the partial wave function overlap between LUMO and HOMO leads to a strong Coulomb interaction, which favors hole transport. From calculation, similar HOMO levels are observed for TET and spiro-OMeTAD, while the LUMO level of TET is about 0.31 eV lower in energy than that of spiro-OMeTAD. The energy level alignment from this calculation agrees well with that from CV results. The calculated hole reorganization energy (λ_{hole}) of TET (112 meV) is smaller than that of spiro-OMeTAD (148 meV),^[50] as shown in Figure S14, Supporting Information, suggesting that TET may have a higher hole mobility than spiro-OMeTAD.

Figure 2a shows a representative cross-sectional scanning electron microscopy (SEM) image of our complete regular planar PVSCs with a structure of FTO/SnO₂/C₆₀-SAM/perovskite/TET/Au, clearly showing a pinhole-free perovskite absorber of \approx 500 nm and a TET layer of \approx 30 nm that is uniformly and conformably coated on the perovskite layer. The optimum thickness of TET layer in our work is only about 30 nm (Figure S15a, Supporting Information), significantly lower than that of a typical spiro-OMeTAD layer (200 nm), as shown in Figure S15b, Supporting Information. The perovskite layer features morphology with large grains and a smooth surface, with a surface roughness of 10.4 nm, as shown in tapping-mode atomic force microscopy (AFM) images (Figure S16, Supporting Information). Upon deposition of the relatively thick spiro-OMeTAD, the surface roughness is reduced to 2.23 nm, indicating that the surface becomes flattened by the accumulation of the spiro-OMeTAD during deposition. For relatively thin TET (around 30 nm) coating, the surface topography is also flattened, although to a less extent, resulting in a slightly higher roughness of 3.97 nm, compared with thick spiro-OMeTAD coating. The functionalities of other layers can be found in our previous publications.^[13,51-54] Figure 2b shows the energy level diagram of our PVSCs with TET or spiro-OMeTAD HSLs.

Figure 3a and b shows the current density-voltage (J - V) curves and external quantum efficiency (EQE) spectra of our best-performing PVSCs with TET and spiro-OMeTAD HSLs under 100 mW cm⁻² AM1.5G illumination. Our champion PVSC with TET HSL achieves a maximum PCE of 19.1% with a V_{oc} of 1.070 V, a J_{sc} of 21.96 mA cm⁻², and a FF of 81.4% under reverse voltage scan, which are comparable with the device performance

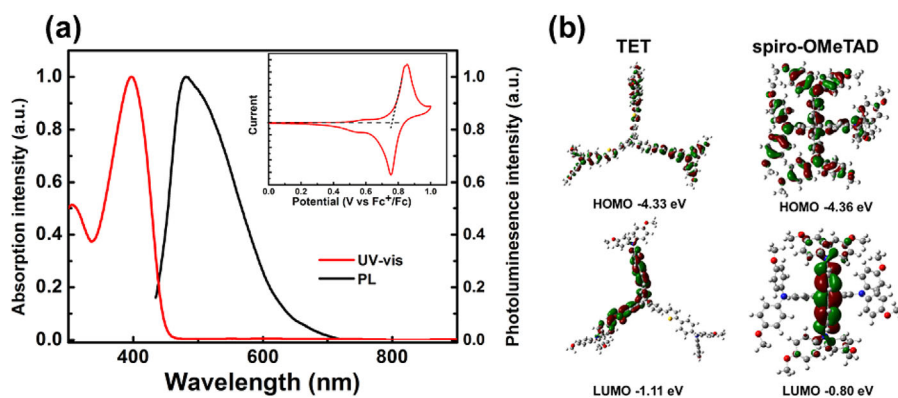


Figure 1. a) Absorption and PL spectra of a TET film. Inset shows cyclic voltammograms of TET with ferrocene as the reference. b) DFT-calculated electronic structures of TET and spiro-OMeTAD, displaying the electronic energy levels of HOMO and LUMO.

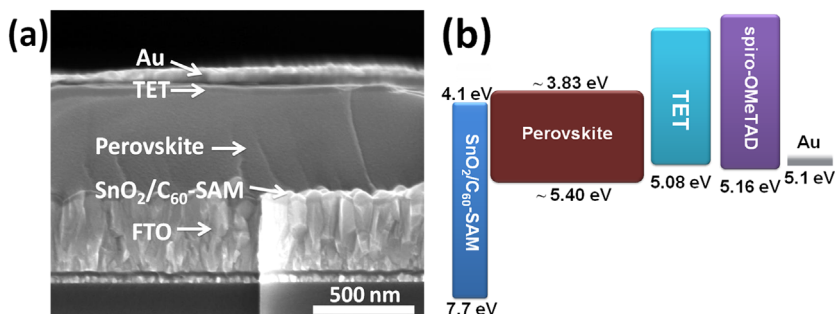


Figure 2. a) Cross-sectional SEM image of our complete regular planar PVSC with TET as HTM. b) Energy level diagram of our regular planar PVSC with TET or spiro-OMeTAD as HSLs.

of our best reference PVSC using spiro-OMeTAD HSL, that is, a PCE of 19.5% with a V_{oc} of 1.123 V, a J_{sc} of 21.90 mA cm^{-2} , and a FF of 79.1%. The EQE-integrated J_{sc} of TET (spiro-OMeTAD) based PVSC over a 100 mW cm^{-2} AM1.5G solar spectrum can reach 21.85 (21.90) mA cm^{-2} , which is in good agreement with those obtained from the J - V curves. It is worth noting that the EQE spectra of devices with TET and spiro-OMeTAD present obvious difference in the wavelength range of 650–750 nm, which is primarily attributed to optical cavity effect caused by the different HSL thicknesses.^[54,55] Our PVSCs with both TET and spiro-OMeTAD HSLs show a small degree of J - V hysteresis behavior, as shown in Figure S17a, Supporting Information. The origin of J - V hysteresis might be ascribed to the perovskite layer itself such as trap states,^[56] ion migration,^[57] or ESL/perovskite interface,^[13,14] although C_{60} -SAM has been applied here in order to reduce the hysteresis. Therefore, we have additionally performed a steady-state efficiency measurement to evaluate

the actual operating performance of the champion PVSC using TET HSL. Its steady-state photocurrent at a constant bias of 0.898 V for 600 s under 100 mW cm^{-2} AM1.5G illumination is $\approx 20.7 \text{ mA cm}^{-2}$, corresponding to a stabilized output power of $\approx 18.6\%$, as shown in Figure 3c, comparable with the steady-state efficiency of $\approx 19.0\%$ for our champion PVSC with spiro-OMeTAD HSL (Figure S17b, Supporting Information). The steady-state efficiency is close to the PCE obtained from J - V curves. The un-encapsulated PVSCs with TET and spiro-OMeTAD as HSLs have been measured under continuous illumination for 2 h at the conditions

(60% humidity and room temperature) by tracking the maximum output power point (Figure S17c, Supporting Information). The PVSC with TET HSLs shows a stability comparable to that with spiro-OMeTAD HSLs, indicating that TET is stable under continuous illumination.^[58] To assess the reproducibility of our devices with TET HSLs, we fabricated 25 devices comprised of several different batches. As shown in the PCE histogram of the corresponding device data (Figure 3d), the average PCE is $18.8 \pm 0.1\%$ with an average V_{oc} of $1.067 \pm 0.005 \text{ V}$, an average J_{sc} of $21.82 \pm 0.45 \text{ mA cm}^{-2}$, and an average FF of $80.6 \pm 0.9\%$ under reverse voltage scan. The PVSCs using spiro-OMeTAD HSLs showed an average PCE of $19.0 \pm 0.3\%$ with an average V_{oc} of $1.108 \pm 0.008 \text{ V}$, an average J_{sc} of $21.95 \pm 0.13 \text{ mA cm}^{-2}$, and an average FF of $78.3 \pm 1.0\%$ under reverse voltage scan. The PCE histogram of the corresponding data is shown in Figure S18, Supporting Information.

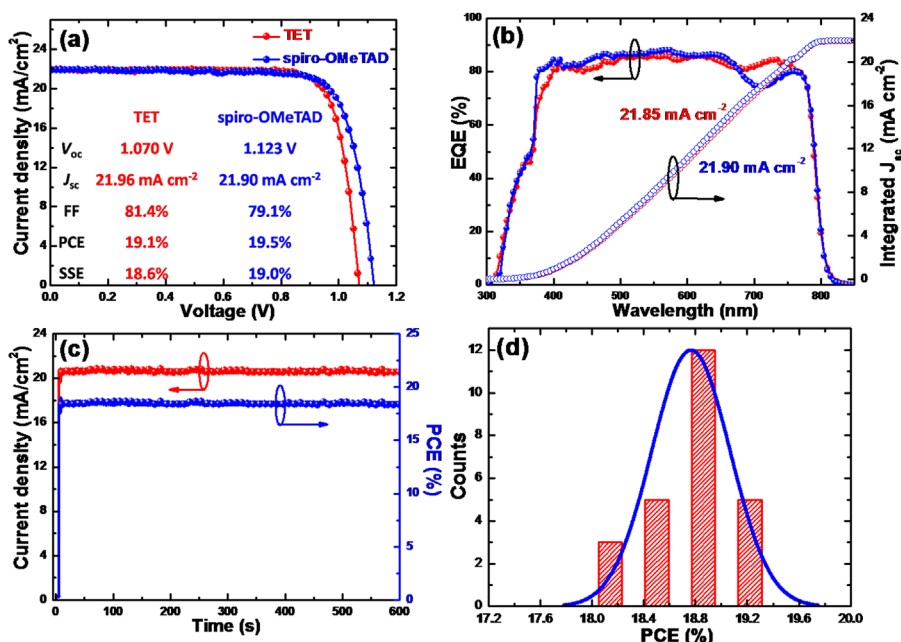


Figure 3. a) J - V curves under 100 mW cm^{-2} AM1.5G illumination measured under reverse voltage scan, b) EQE spectra and integrated J_{sc} s, of our best-performing PVSCs with TET and spiro-OMeTAD HSLs; c) Steady-state photocurrent and PCE at a constant bias of 0.898 V of our best-performing PVSC with TET HSLs; d) Histogram of PCEs measured for 25 cells using TET-based PVSCs.

The above results show that the PCE difference between TET-based and spiro-OMeTAD-based PVSCs mainly originates from the differences in V_{oc} and FF. The average V_{oc} (1.067 ± 0.005 V) of TET-based PVSCs is slightly smaller than that (1.108 ± 0.008 V) of spiro-OMeTAD-based PVSCs, which can be primarily attributed to the higher HOMO of TET (-5.08 eV) than that of spiro-OMeTAD (-5.16 eV). The TET-based PVSCs exhibit extremely high average FFs of over 80%, with a FF of 81.4% for the champion cell.

To understand the origin of the high FF, steady-state photoluminescence (PL) and time resolved photoluminescence (TRPL) measurements were performed to evaluate the charge transfer at the perovskite/HSL interface. As shown in Figure S19, Supporting Information, the deposition of either TET or spiro-OMeTAD quenches the PL intensity of perovskite films, however, TET quenches more than spiro-OMeTAD, indicating a better charge transfer at the perovskite/TET interface than at the perovskite/spiro-OMeTAD interface. The charge carrier dynamics characterized by TRPL decay is also found to be shortened in case of perovskite film coated with TET (mean carrier lifetime = 39 ns) relative to the case of perovskite film coated with spiro-OMeTAD (mean carrier lifetime = 99 ns) and the case of the pristine perovskite film (mean carrier lifetime = 623 ns) as depicted in **Figure 4a**, confirming a faster charge transfer at the perovskite/TET interface. Meanwhile, a thin layer of TET on perovskite is compact and uniform with a complete coverage as evidenced by cross-sectional SEM and perspective-view AFM images (Figure 2a and Figure S16c, Supporting Information), which suppresses the charge recombination at the perovskite/HSL/Au interface. Indeed, the measured trap density of states (tDOS) show that TET-based PVSC has a slightly lower trap density than the spiro-OMeTAD-based PVSC, as shown in Figure 4b.

Figure S20, Supporting Information, shows the Nyquist plots of the PVSCs with TET and spiro-OMeTAD HSLs measured from electrochemical impedance spectroscopy (EIS). The Nyquist plot for each device shows two semicircles, in which the first one at higher frequency region (lower impedance value of the Nyquist plot) is ascribed to the impedance predominated by the charge transport and recombination kinetics and the second one at lower frequency region (higher impedance value of the Nyquist plot) is ascribed to the speed of ions' relaxation/diffusion.^[59–61] At a bias of 0V, the first semicircle (higher

frequency region) of the Nyquist plot is associated with the recombination resistance (R_{rec}) at the perovskite/charge selective layer. Since both of these devices have the same ESL/perovskite interface, any differences in the R_{rec} values should be attributed to the HSL/perovskite interface. The PVSC with TET HSL shows a higher R_{rec} value than that with spiro-OMeTAD HSL, indicating a reduction in recombination loss, partially contributing to the slightly higher FF in PVSC with TET HSL.

Carrier mobility of HSL materials is crucial for the charge carrier balance in the planar PVSCs.^[14,28] We find that TET exhibits a higher hole mobility than spiro-OMeTAD. We used hole-only devices with the configuration of ITO/ poly(3,4-ethylenedioxythiophene):polystyrene sulfonate (PEDOT:PSS)/TET or spiro-OMeTAD/MoO₃/Ag to evaluate charge mobilities by space charge-limited currents (SCLC) model.^[5] The carrier mobility was determined by fitting modified Mott–Gurney equation taking the electric field and temperature dependence into account as described below,^[62]

$$J = \frac{9}{8} \epsilon_0 \epsilon_r \mu \left[0.89 \beta(T) \sqrt{\frac{V}{d}} \right] \frac{V^2}{d^3}$$

where J is the dark current density, μ is the zero-field mobility, V is the effective voltage ($V = V_{Applied} - V_{Built-in} - V_{series\ resistanc}$), ϵ_0 is the vacuum permittivity, ϵ_r is the dielectric constant of the HTM (here $\epsilon_r = 3$),^[63] and d is the thickness of HSL films. The hole mobility values are estimated to be $5.4 \times 10^{-4} \text{ cm}^2 \text{ V}^{-1} \text{ s}^{-1}$ and $8.2 \times 10^{-4} \text{ cm}^2 \text{ V}^{-1} \text{ s}^{-1}$ for spiro-OMeTAD and TET, respectively, as shown in Figure S21, Supporting Information. A higher hole mobility leads to a better hole transport, which decreases the imbalance of charge transport in a planar PVSC. Additionally, a thinner HSL can transport holes more effectively and further reduce the imbalance of charge transport. These are the primary reasons for the high FFs obtained in PVSCs using TET HSLs. The increase in charge mobility can be attributed to the lower internal reorganization energy of TET, which was calculated to be 112 meV that is smaller than that of spiro-OMeTAD (148 meV), as shown in Figure S14, Supporting Information. The hole mobility can be dominated by the reorganization energy without regard for the electronic coupling, that is, a smaller hole reorganization energy benefits a higher hole mobility.^[50] Moreover, high hole mobility of TET might be

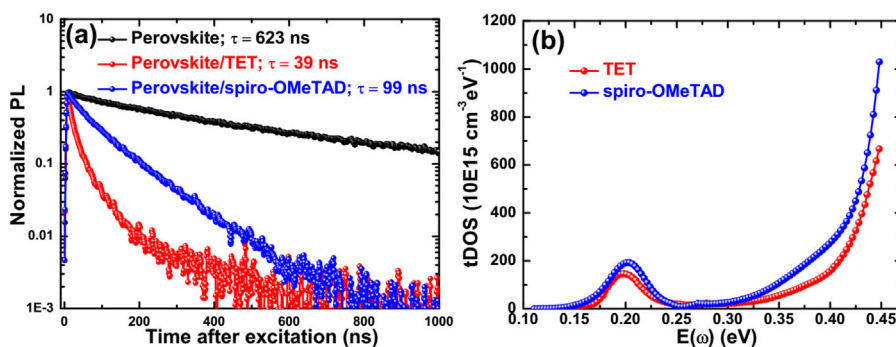


Figure 4. a) TRPL decay of perovskite film, perovskite/spiro-OMeTAD, and perovskite/TET. b) trap density of states of PVSCs with TET and spiro-OMeTAD HSLs.

ascribed to the 3D conjugated structure, facilitating hole transport through this thin TET HSL. Thus, our results suggest that the full coverage of very thin TET layer on perovskite, fast, and efficient charge transfer as well as high hole mobility are responsible for the high FFs of PVSCs using TET HSLs.

3. Conclusion

In summary, we have synthesized and characterized a new HSL material, that is, TET, which inherits excellent optoelectronic properties and overcomes the major shortfalls of the most popular HSL material, that is, spiro-OMeTAD. Planar PVSCs using TET HSLs achieved a maximum PCE of 19.1% under reverse voltage scan and a steady-state efficiency of 18.6%, comparable with those (19.5% PCE and 19.0% steady-state efficiency) of the best PVSC using spiro-OMeTAD HSL. Importantly, our efficient PVSCs used very thin TET HSLs (about 30 nm), exhibiting good stability under continuous illumination. Considering the lower laboratory synthesis and purification cost (\$123 vs. \$500 g⁻¹) and thinner HSL (30 vs. 200 nm), the cost for TET on a unit area of one device is significantly lower (25 times) than that for high-purity spiro-OMeTAD. Therefore, our work moves a significant step forward toward the commercialization of the emerging PVSC technology.

4. Experimental Section

Solution Preparation: MA_{0.7}FA_{0.3}PbI₃ precursor: Lead iodide (PbI₂, Alfa Aesar), methylammonium iodide (MAI, Dyesol), formamidinium iodide (FAI, Dyesol), lead thiocyanate (Pb(SCN)₂, Sigma-Aldrich, 99.5%), dimethyl sulfoxide (DMSO, Sigma-Aldrich), and N,N-dimethylformamide (DMF, Sigma-Aldrich) were used as purchased. The perovskite precursor was prepared using a Lewis acid-base adduct approach with the mixture of MAI, FAI, PbI₂, DMSO, and Pb(SCN)₂ in DMF. The details have been described in our previous papers.^[13,14] A small amount of Pb(SCN)₂ was added as the additive.^[13,14,51,53] The precursor solution was stirred on a hotplate at 60 °C before deposition. The FAPbI₃ precursor solution was made in the same process. The MA_{0.7}FA_{0.3}PbI₃ precursor was prepared by mixing two solutions together. The resulted precursor was stirred and then purified using a 0.45 μm filter before spin-coating.

Spiro-OMeTAD: 2,2',7,7'-Tetrakis(N,N'-di-p-methoxyphenylamine)-9,9'-spirobifluorene (spiro-OMeTAD) was used as the HSL and deposited on the perovskite film at 2000 rpm for 60 s. The spiro-OMeTAD was co-doped using Co-TFSI and Li-TFSI. The Spiro-OMeTAD solution was prepared by dissolving 72.3 mg Spiro-OMeTAD (Shenzhen Feiming Science and Technology Co., Ltd.) in 1 mL chlorobenzene (CB) with 28 μL 4-tert-butylpyridine (tBP) (Sigma-Aldrich), 18 μL Li-bis-(trifluoromethanesulfonyl) imide (Li-TFSI) (Sigma-Aldrich) (520 mg mL⁻¹ in acetonitrile) and 18 μL Co(II)-TFSI salt (FK102, Dyesol) (300 mg mL⁻¹ in acetonitrile).

TET: A solution of TET/toluene (10 mg mL⁻¹) with an additive of 7.5 μL Li-TFSI (170 mg mL⁻¹ in acetonitrile) and 4 μL tBP was spin-coated on perovskite layer at 3000 rpm for 45 s.

Device Fabrication: The FTO substrates were cleaned by ultrasonication in diluted Micro-90 detergent, deionized water, acetone, and isopropanol for 15 min, respectively. SnO₂ layer was deposited on the FTO using plasma-enhanced atomic layer deposition (PEALD) method.^[13,14,52] The SnO₂ layer was annealed at 100 °C for 1 h in ambient air under the conditions that the room temperature was about 25 °C and the humidity was about 55%. C₆₀-SAM has the concentration of 4 mg mL⁻¹ in chlorobenzene (Sigma-Aldrich, 99.8%). The C₆₀-SAM solution was then spin-coated onto the SnO₂ layer at 3000 rpm for 1 min. The perovskite precursor solution was spin-coated on the PEALD SnO₂

layer at 500 rpm for 3 s and at 4000 rpm for 60 s using the anti-solvent technique. Diethyl ether, as the anti-solvent agent, was then drop-cast on the substrate. After spin coating, the perovskite film was annealed at 100 °C for 5 min. All of these processes were carried out in a N₂ filled glove box. Spiro-OMeTAD was deposited on the perovskite film at 2000 rpm for 60 s. The Spiro-OMeTAD was co-doped using Co-TFSI and Li-TFSI as reported previously.^[64] The TET doped with Li-TFSI was spin-coated on the perovskite film at 3000 rpm for 60 s, resulting in an ≈30 nm layer. A layer of 80 nm gold (Au) was then deposited on the top of spiro-OMeTAD using thermal evaporation. The working area of the devices was 0.08 cm² as defined by a shadow mask during the Au evaporation. For hole-only devices, a 30 nm PEDOT:PSS layer was spin-coated on ITO substrate, followed by the deposition of TET or spiro-OMeTAD layer in a glove box. Then, 8 nm MoO₃ and 75 nm Ag layers were thermally evaporated to finish the device fabrication.

Material, Film, and Device Characterization: TET Synthesis and Characterization: Commercially available reagents were purchased from Sigma-Aldrich and used without further purification. Toluene and Tetrahydrofuran (THF) were freshly distilled before use. Other solvents were used directly. ¹H NMR and ¹³C NMR spectra were recorded on Bruker AVANCE III 500 MHz spectrometer with tetramethylsilane (TMS) as internal standard. Mass spectra were obtained by Bruker ultrafleXtreme MALDITOF/TOF. The absorption spectra were measured by UV-Vis spectrophotometer (PerkinElmer Lambda 1050). Photoluminescence (PL) spectra were recorded on Horiba Jobin Yvon Model FM-4NIR spectrophotometer in Figure 1a. The electrochemical cyclic voltammetry (CV) was conducted on an electrochemical workstation (CHI660D Chenhua Shanghai) with Pt plate as working electrode, Pt slice as counter electrode, and Ag/AgCl electrode as reference electrode in tetrabutylammonium hexafluorophosphate (Bu₄NPF₆, 0.1 M) acetonitrile solutions at a scan rate of 50 mV s⁻¹. Ferrocene/ferrocenium (Fc/Fc⁺) was used as the internal standard (the energy level of Fc/Fc⁺ is -4.8 eV under vacuum),^[65] and the formal potential of Fc/Fc⁺ was measured as 0.48 V versus Ag/AgCl electrode. The HOMO energy level was determined from the onset oxidation (E_{onset}^{ox}) as HOMO = -4.8 - 0.48 + E_{onset}^{ox} (eV); while the LUMO energy level was calculated with HOMO and optical bandgap (E_g) by the formula as: LUMO = HOMO + E_g (eV). Thermogravimetric analysis (TGA) was conducted on TGA/SDTA851E (Mettler Toledo) under nitrogen atmosphere at a heating rate of 20 °C min⁻¹ from 50 °C to 800 °C. The instrument type was TGA/SDTA851E (Mettler Toledo).

Film Characterization: High resolution field emission top-view and cross-sectional SEM images of all films and completed devices were taken with Hitachi S-4800. Atomic force microscopy (AFM) images were acquired on a Veeco Nanoscope IIIA instrument operated in the tapping mode with a 1 Ω etched silicon wafer probe (Bruker). All layer thicknesses were determined using a Dektak surface profiler and cross-sectional SEM images. PL measurements (Figure S19, Supporting Information) were conducted similarly as described in our earlier works.^[52,66] Samples were illuminated through the glass side. A 532 nm cw laser at 115 mW cm⁻² was used as a source of excitation for steady-state PL while 532 nm pulsed laser at ≈10⁹ photons · pulse⁻¹ cm⁻² was used as a source of excitation in TRPL measurement (Figure 4a). PL decay curves were biexponential in nature and fitted by iterative re-convolution with the measured system response function. Mean photogenerated carrier lifetimes for the biexponential fit is calculated by the weighted average method.^[52]

Device Characterization: J-V curves were measured in air under 100 mW cm⁻² AM1.5G solar irradiation (PV Measurements Inc.) with a Keithley 2400 Source Meter. The incident light was controlled by a shutter. The light intensity for J-V measurements was calibrated by a standard Si solar cell and our perovskite solar cells certified by Newport.^[12] The steady-state efficiencies were obtained by tracking the maximum output power point. The stability of un-encapsulated PVSCs with TET and spiro-OMeTAD as HSLs was taken under continuous illumination at the conditions of 60% humidity and room temperature by tracking the maximum output power point. EQE spectra were performed on a QE system (PV Measurements Inc., model IVQE8-C QE system without bias voltage) using 100 Hz chopped monochromatic light ranging from 300 to 850 nm under

near-dark test conditions. Electrochemical impedance spectroscopy, used to obtain both the Nyquist diagram and the trap density of states plots, were performed using a Solartron Modulab potentiost/galvanostat equipped with a 1 MHz frequency response analyzer module. The devices were held at 0 V bias in dark while a 10 mV potential perturbation was applied at frequencies ranging from 1 MHz to 10 mHz. All characterizations and measurements were performed in the ambient.

Supporting Information

Supporting Information is available from the Wiley Online Library or from the author.

Acknowledgements

YS, CW, and DZ contributed equally to this work. The design and development of TET was completed by Tang's group at Nanjing University of Science and Technology under the financial support from the National Natural Science Foundation of China (Grant No. 51573077), the Jiangsu Province Natural Science Foundation for Distinguished Young Scholars (BK20130032), the Program for New Century Excellent Talents in University (NCET-12-0633), and the Priority Academic Program Development of Jiangsu Higher Education Institutions. This work is financially supported by the U.S. Department of Energy (DOE) SunShot Initiative under the Next Generation Photovoltaics 3 program (DE-FOA-0000990), National Science Foundation under contract no. CHE-1230246 and DMR-1534686, and the Ohio Research Scholar Program.

Conflict of Interest

The authors declares no conflict of interest.

Keywords

charge transfer, hole selective layers, hole transport materials, perovskite solar cells, TET

Received: October 19, 2017

Revised: November 22, 2017

Published online: December 21, 2017

- [1] D. B. Mitzi, S. Wang, C. A. Feild, C. A. Chess, A. M. Guloy, *Science* **1995**, 267, 1473.
- [2] S. D. Stranks, G. E. Eperon, G. Grancini, C. Menelaou, M. J. P. Alcocer, T. Leijtens, L. M. Herz, A. Petrozza, H. J. Snaith, *Science* **2013**, 342, 341.
- [3] W.-J. Yin, T. Shi, Y. Yan, *Adv. Mater.* **2014**, 26, 4653.
- [4] W.-J. Yin, T. Shi, Y. Yan, *Appl. Phys. Lett.* **2014**, 104, 063903.
- [5] Q. Dong, Y. Fang, Y. Shao, P. Mulligan, J. Qiu, L. Cao, J. Huang, *Science* **2015**, 347, 967.
- [6] B. Saparov, D. B. Mitzi, *Chem. Rev.* **2016**, 116, 4558.
- [7] A. Kojima, K. Teshima, Y. Shirai, T. Miyasaka, *J. Am. Chem. Soc.* **2009**, 131, 6050.
- [8] W. S. Yang, J. H. Noh, N. J. Jeon, Y. C. Kim, S. Ryu, J. Seo, S. I. Seok, *Science* **2015**, 348, 1234.
- [9] N. Ahn, D.-Y. Son, I.-H. Jang, S. M. Kang, M. Choi, N.-G. Park, *J. Am. Chem. Soc.* **2015**, 137, 8696.
- [10] D. Bi, C. Yi, J. Luo, J.-D. Décoppet, F. Zhang, S. M. Zakeeruddin, X. Li, A. Hagfeldt, M. Grätzel, *Nat. Energy* **2016**, 1, 16142.
- [11] M. Yang, Z. Li, M. O. Reese, O. G. Reid, D. H. Kim, S. Siol, T. R. Klein, Y. Yan, J. J. Berry, M. F. A. M. van Hest, K. Zhu, *Nat. Energy* **2017**, 2, 17038.
- [12] D. Zhao, Y. Yu, C. Wang, W. Liao, N. Shrestha, C. R. Grice, A. J. Cimaroli, L. Guan, R. J. Ellingson, K. Zhu, X. Zhao, R.-G. Xiong, Y. Yan, *Nat. Energy* **2017**, 2, 17018.
- [13] C. Wang, D. Zhao, Y. Yu, N. Shrestha, C. R. Grice, W. Liao, A. J. Cimaroli, J. Chen, R. J. Ellingson, X. Zhao, Y. Yan, *Nano Energy* **2017**, 35, 223.
- [14] C. Wang, C. Xiao, Y. Yu, D. Zhao, R. A. Awani, C. R. Grice, K. Ghimire, D. Constantinou, W. Liao, A. J. Cimaroli, P. Liu, J. Chen, N. J. Podraza, C.-S. Jiang, M. M. Al-Jassim, X. Zhao, Y. Yan, *Adv. Energy Mater.* **2017**, 7, 1700414.
- [15] H.-S. Kim, C.-R. Lee, J.-H. Im, K.-B. Lee, T. Moehl, A. Marchioro, S.-J. Moon, R. Humphry-Baker, J.-H. Yum, J. E. Moser, M. Grätzel, N.-G. Park, *Sci. Rep.* **2012**, 2, 591.
- [16] Y. Zhou, M. Yang, W. Wu, A. L. Vasiliev, K. Zhu, N. P. Padture, *J. Mater. Chem. A* **2015**, 3, 8178.
- [17] M. Yang, Y. Zhou, Y. Zeng, C.-S. Jiang, N. P. Padture, K. Zhu, *Adv. Mater.* **2015**, 27, 6363.
- [18] F. Fu, T. Feurer, T. Jäger, E. Avancini, B. Bissig, S. Yoon, S. Buecheler, A. N. Tiwari, *Nat. Commun.* **2015**, 6, 8932.
- [19] F. Fu, T. Feurer, T. P. Weiss, S. Pisoni, E. Avancini, C. Andres, S. Buecheler, A. N. Tiwari, *Nat. Energy* **2016**, 2, 16190.
- [20] N. Wang, L. Cheng, R. Ge, S. Zhang, Y. Miao, W. Zou, C. Yi, Y. Sun, Y. Cao, R. Yang, Y. Wei, Q. Guo, Y. Ke, M. Yu, Y. Jin, Y. Liu, Q. Ding, D. Di, L. Yang, G. Xing, H. Tian, C. Jin, F. Gao, R. H. Friend, J. Wang, W. Huang, *Nat. Photon.* **2016**, 10, 699.
- [21] S. Zhang, C. Yi, N. Wang, Y. Sun, W. Zou, Y. Wei, Y. Cao, Y. Miao, R. Li, Y. Yin, N. Zhao, J. Wang, W. Huang, *Adv. Mater.* **2017**, 29, 160660.
- [22] Z. Xiao, R. A. Kerner, L. Zhao, N. L. Tran, K. M. Lee, T.-W. Koh, G. D. Scholes, B. P. Rand, *Nat. Photon.* **2017**, 11, 108.
- [23] L. Shen, Y. Fang, D. Wang, Y. Bai, Y. Deng, M. Wang, Y. Lu, J. Huang, *Adv. Mater.* **2016**, 28, 10794.
- [24] Y. Fang, Q. Dong, Y. Shao, Y. Yuan, J. Huang, *Nat. Photon.* **2015**, 9, 679.
- [25] H. Zhu, Y. Fu, F. Meng, X. Wu, Z. Gong, Q. Ding, M. V. Gustafsson, M. T. Trinh, S. Jin, X. Y. Zhu, *Nat. Mater.* **2015**, 14, 636.
- [26] L. Calió, S. Kazim, M. Grätzel, S. Ahmad, *Angew. Chem. Int. Ed.* **2016**, 55, 14522.
- [27] W. Yan, S. Ye, Y. Li, W. Sun, H. Rao, Z. Liu, Z. Bian, C. Huang, *Adv. Energy Mater.* **2016**, 6, 1600474.
- [28] K. Chen, Q. Hu, T. Liu, L. Zhao, D. Luo, J. Wu, Y. Zhang, W. Zhang, F. Liu, T. P. Russell, R. Zhu, Q. Gong, *Adv. Mater.* **2016**, 28, 10718.
- [29] L. Guan, X. Yin, D. Zhao, C. Wang, Q. An, J. Yu, N. Shrestha, C. R. Grice, R. A. Awani, Y. Yu, Z. Song, J. Zhou, W. Meng, F. Zhang, R. J. Ellingson, J. Wang, W. Tang, Y. Yan, *J. Mater. Chem. A* **2017**, 5, 23319.
- [30] T. Liu, K. Chen, Q. Hu, R. Zhu, Q. Gong, *Adv. Energy Mater.* **2016**, 6, 1600457.
- [31] X. Yin, L. Guan, J. Yu, D. Zhao, C. Wang, N. Shrestha, Y. Han, Q. An, J. Zhou, B. Zhou, Y. Yu, C. R. Grice, R. A. Awani, F. Zhang, J. Wang, R. J. Ellingson, Y. Yan, W. Tang, *Nano Energy* **2017**, 40, 163.
- [32] M. Saliba, S. Orlandi, T. Matsui, S. Aghazada, M. Cavazzini, J.-P. Correa-Baena, P. Gao, R. Scopelliti, E. Mosconi, K.-H. Dahmen, F. De Angelis, A. Abate, A. Hagfeldt, G. Pozzi, M. Graetzel, M. K. Nazeeruddin, *Nat. Energy* **2016**, 1, 15017.
- [33] Q. Jiang, L. Zhang, H. Wang, X. Yang, J. Meng, H. Liu, Z. Yin, J. Wu, X. Zhang, J. You, *Nat. Energy* **2016**, 2, 16177.
- [34] S. S. Shin, E. J. Yeom, W. S. Yang, S. Hur, M. G. Kim, J. Im, J. Seo, J. H. Noh, S. I. Seok, *Science* **2017**, 356, 167.
- [35] Q. Wang, Q. Dong, T. Li, A. Gruverman, J. Huang, *Adv. Mater.* **2016**, 28, 6734.
- [36] Y. Shao, Y. Yuan, J. Huang, *Nat. Energy* **2016**, 1, 15001.

- [37] B. Xu, D. Bi, Y. Hua, P. Liu, M. Cheng, M. Gratzel, L. Kloo, A. Hagfeldt, L. Sun, *Energy Environ. Sci.* **2016**, *9*, 873.
- [38] T. Malinauskas, M. Saliba, T. Matsui, M. Daskeviciene, S. Urnikaite, P. Gratia, R. Send, H. Wonneberger, I. Bruder, M. Gratzel, V. Getautis, M. K. Nazeeruddin, *Energy Environ. Sci.* **2016**, *9*, 1681.
- [39] C. Huang, W. Fu, C.-Z. Li, Z. Zhang, W. Qiu, M. Shi, P. Heremans, A. K. Y. Jen, H. Chen, *J. Am. Chem. Soc.* **2016**, *138*, 2528.
- [40] H. Zhang, J. Cheng, F. Lin, H. He, J. Mao, K. S. Wong, A. K. Y. Jen, W. C. H. Choy, *ACS Nano* **2016**, *10*, 1503.
- [41] J. W. Jung, C.-C. Chueh, A. K. Y. Jen, *Adv. Mater.* **2015**, *27*, 7874.
- [42] P. Qin, S. Tanaka, S. Ito, N. Tetreault, K. Manabe, H. Nishino, M. K. Nazeeruddin, M. Grätzel, *Nat. Commun.* **2014**, *5*, 3834.
- [43] S. Ye, H. Rao, W. Yan, Y. Li, W. Sun, H. Peng, Z. Liu, Z. Bian, Y. Li, C. Huang, *Adv. Mater.* **2016**, *28*, 9648.
- [44] J. A. Christians, R. C. M. Fung, P. V. Kamat, *J. Am. Chem. Soc.* **2013**, *136*, 758.
- [45] A. T. Murray, J. M. Frost, C. H. Hendon, C. D. Molloy, D. R. Carbery, A. Walsh, *Chem. Commun.* **2015**, *51*, 8935.
- [46] N. Marinova, W. Tress, R. Humphry-Baker, M. I. Dar, V. Bojinov, S. M. Zakeeruddin, M. K. Nazeeruddin, M. Grätzel, *ACS Nano* **2015**, *9*, 4200.
- [47] U. B. Cappel, T. Daeneke, U. Bach, *Nano Lett.* **2012**, *12*, 4925.
- [48] W. H. Nguyen, C. D. Bailie, E. L. Unger, M. D. McGehee, *J. Am. Chem. Soc.* **2014**, *136*, 10996.
- [49] P. Gao, M. Gratzel, M. K. Nazeeruddin, *Energy Environ. Sci.* **2014**, *7*, 2448.
- [50] A. Krishna, D. Sabba, H. Li, J. Yin, P. P. Boix, C. Soci, S. G. Mhaisalkar, A. C. Grimsdale, *Chem. Sci.* **2014**, *5*, 2702.
- [51] W. Ke, C. Xiao, C. Wang, B. Saparov, H.-S. Duan, D. Zhao, Z. Xiao, P. Schulz, S. P. Harvey, W. Liao, W. Meng, Y. Yu, A. J. Cimaroli, C.-S. Jiang, K. Zhu, M. Al-Jassim, G. Fang, D. B. Mitzi, Y. Yan, *Adv. Mater.* **2016**, *28*, 5214.
- [52] C. Wang, D. Zhao, C. R. Grice, W. Liao, Y. Yu, A. Cimaroli, N. Shrestha, P. J. Roland, J. Chen, Z. Yu, P. Liu, N. Cheng, R. J. Ellingson, X. Zhao, Y. Yan, *J. Mater. Chem. A* **2016**, *4*, 12080.
- [53] Y. Yu, C. Wang, C. R. Grice, N. Shrestha, J. Chen, D. Zhao, W. Liao, A. J. Cimaroli, P. J. Roland, R. J. Ellingson, Y. Yan, *ChemSusChem* **2016**, *9*, 3288.
- [54] D. Zhao, W. Ke, C. R. Grice, A. J. Cimaroli, X. Tan, M. Yang, R. W. Collins, H. Zhang, K. Zhu, Y. Yan, *Nano Energy* **2016**, *19*, 88.
- [55] Q. Lin, A. Armin, R. C. R. Nagiri, P. L. Burn, P. Meredith, *Nat. Photon.* **2015**, *9*, 106.
- [56] Y. Shao, Z. Xiao, C. Bi, Y. Yuan, J. Huang, *Nat. Commun.* **2014**, *5*, 5784.
- [57] B. Chen, M. Yang, X. Zheng, C. Wu, W. Li, Y. Yan, J. Bisquert, G. Garcia-Belmonte, K. Zhu, S. Priya, *J. Phys. Chem. Lett.* **2015**, *6*, 4693.
- [58] T. A. Berhe, W.-N. Su, C.-H. Chen, C.-J. Pan, J.-H. Cheng, H.-M. Chen, M.-C. Tsai, L.-Y. Chen, A. A. Dubale, B.-J. Hwang, *Energy Environ. Sci.* **2016**, *9*, 323.
- [59] M. Bag, L. A. Renna, R. Y. Adhikari, S. Karak, F. Liu, P. M. Lahti, T. P. Russell, M. T. Tuominen, D. Venkataraman, *J. Am. Chem. Soc.* **2015**, *137*, 13130.
- [60] Y. Liu, M. Bag, L. A. Renna, Z. A. Page, P. Kim, T. Emrick, D. Venkataraman, T. P. Russell, *Adv. Energy Mater.* **2016**, *6*, 1501606.
- [61] Y. Liu, L. A. Renna, Z. A. Page, H. B. Thompson, P. Y. Kim, M. D. Barnes, T. Emrick, D. Venkataraman, T. P. Russell, *Adv. Energy Mater.* **2016**, *6*, 1600664.
- [62] P. N. Murgatroyd, *J. Phys. D Appl. Phys.* **1970**, *3*, 151.
- [63] Z. Li, K. Jiang, G. Yang, J. Y. L. Lai, T. Ma, J. Zhao, W. Ma, H. Yan, *Nat. Commun.* **2016**, *7*, 13094.
- [64] D. Bi, W. Tress, M. I. Dar, P. Gao, J. Luo, C. Renevier, K. Schenk, A. Abate, F. Giordano, J.-P. C. Baena, *Sci. Adv.* **2016**, *2*, e1501170.
- [65] Z. Chen, M. G. Debije, T. Debaerdemaeker, P. Osswald, F. Würthner, *ChemPhysChem* **2004**, *5*, 137.
- [66] W. Liao, D. Zhao, Y. Yu, N. Shrestha, K. Ghimire, C. R. Grice, C. Wang, Y. Xiao, A. J. Cimaroli, R. J. Ellingson, N. J. Podraza, K. Zhu, R.-G. Xiong, Y. Yan, *J. Am. Chem. Soc.* **2016**, *138*, 12360.